

THESIS FOR THE DEGREE OF LICENTIATE OF ENGINEERING

Microstructure and mechanical properties of Ti-6Al-4V welds produced with  
different processes

Sakari Tolvanen



Department of Materials and Manufacturing Technology

CHALMERS UNIVERSITY OF TECHNOLOGY

Gothenburg, Sweden 2016

Microstructure and mechanical properties of Ti-6Al-4V welds produced with different processes

Sakari Tolvanen

© Sakari Tolvanen, 2016

ISSN 1652-8891

Technical report no 109/2016

Department of Materials and Manufacturing Technology

Chalmers University of Technology

SE-412 96 Gothenburg

Sweden

Telephone + 46 (0)31-772 1000

Printed by Chalmers Reproservice

Gothenburg, Sweden 2016

To my parents



# Microstructure and mechanical properties of Ti-6Al-4V welds produced with different processes

Sakari Tolvanen

Department of Materials and Manufacturing Technology  
Chalmers University of Technology

## Abstract

Titanium alloys are widely used for components in the fan and compressor sections of aeroengines mainly because of their superior strength-to-weight ratio. Large static compressor components can be manufactured by welding together smaller subcomponents, which has potential to provide benefits such as higher buy-to-fly ratio and improved performance of the components. This is the background for why welding and the mechanical properties of welds have been investigated in this project. Fusion welding involves localized melting of materials which produces changes in microstructure, geometry of the surface, residual stresses and defects in the material, which all can affect the mechanical properties of weld zones.

In this study, fusion welds have been produced with tungsten inert gas welding (TIG), plasma arc welding (PAW), electron beam welding (EBW) and laser beam welding (LBW) of Ti-6Al-4V sheet material. In addition, investigation of LBW and TIG welds in cast Ti-6Al-4V material with different boron contents have also been performed within this work. The mechanical properties of the different weld types have been evaluated with respect to microhardness, yield strength, ultimate tensile strength, ductility and fatigue at room temperature and at elevated temperatures. Metallographic investigation was carried out to characterize the microstructures of the different weld types and weld zones. The fractographic investigation was conducted in order to relate the effect of defects and microstructure on fatigue performance.

High energy beam welding processes render a finer weld material microstructure in comparison to the coarser microstructure produced by arc welding processes, and finer weld microstructure was found to be beneficial for tensile ductility and low cycle fatigue performance. Porosity was found in all the welds. Fatigue life in arc welds was found to be more sensitive to porosity than the high energy beam welds. Large pores and pores located close to the specimen surface were found to be most detrimental for fatigue strength. The boron addition was found to render a significantly finer prior  $\beta$  grain size, and smaller  $\alpha$  colonies and  $\alpha$  plates in the weld zones, as compared with that of standard Ti-64 welds.

**Keywords:** Ti-6Al-4V, welding, defects, porosity, microstructure, fatigue



## **Preface**

This licentiate thesis is based on the work performed at the Department of Materials and Manufacturing Technology between January 2014 and November 2016. The project has been carried out under the supervision of Professor Uta Klement and Professor Robert Pederson.

The thesis consists of an introductory part followed by the appended papers:

- Paper 1:** Fatigue strength dependence on microstructure and defects in Ti-6Al-4V welds,  
*Proceedings of the World Conference of Titanium, 2015*
- Paper 2:** TIG welding and laser welding of boron alloyed Ti-6Al-4V,  
*Proceedings of the 10th International Conference on Trends in Welding Research, 2016*
- Paper 3:** Comparing microstructure and mechanical properties of Ti-6Al-4V welds produced with different processes, *manuscript*

## **Contribution to the appended papers**

The author planned and performed the microstructure characterisation and the fractographic study, evaluated the results of mechanical testing and wrote the papers together with the co-authors.





## Table of contents

1	Introduction .....	1
1.1	Objective .....	2
2	Background .....	3
2.1	Titanium industry and applications .....	3
2.2	Common titanium alloys and physical metallurgy .....	4
3	Welding of titanium alloys .....	7
3.1	Welding processes .....	7
3.2	Welding metallurgy of Ti-6Al-4V .....	13
3.3	Typical defects in titanium alloy welds .....	15
3.4	Mechanical properties of Ti-6Al-4V welds .....	18
4	Fatigue .....	20
4.1	Fatigue in welds .....	21
4.2	Stress based method for fatigue analysis .....	22
4.3	Effect of weld metal porosity on fatigue .....	23
5	Experimental techniques .....	25
5.1	Materials .....	25
5.2	Welding .....	25
5.3	Microstructural characterization .....	27
5.4	Mechanical testing .....	28
6	Summary of appended papers/experimental results .....	31
6.1	Paper 1 .....	31
6.2	Paper 2 .....	33
6.3	Paper 3 .....	35
6.4	Conclusions .....	37
7	Future work .....	39
8	Acknowledgements .....	41
	References .....	43



# 1 Introduction

This thesis intends to contribute to the understanding of the formation of different microstructures and defects in welding of titanium alloys and the effect of these aspects on mechanical properties of the welds.

Titanium alloys are widely used for components in the fan and compressor sections of aeroengines owing to their high specific strength and creep properties at moderate temperatures. Large static compressor parts are traditionally manufactured from large single piece castings that are machined into final shape. A significant amount of the initial casting weight is machined away in order to achieve the finished geometry. This is neither environmentally friendly nor economically viable. Fabricating these large static compressor components through welding them out of smaller subcomponents instead of machining them from large single piece castings provides several potential benefits. There will be less scrap material and the structure can be designed to be more efficient owing to the possibility of selecting high strength titanium alloys in specific parts of the structure enabling increased functionality and improved performance, in the end resulting in reduced environmental impact. Fabrication technologies however require joining of subcomponents which is why welding and the mechanical properties of welds have been investigated here.

Fusion welding involves localized melting of materials which produces changes and defects in the material, which affect the mechanical properties of weld zones and make the design of fatigue resistant joints a complicated process. These reasons also result in a large statistical scatter in the fatigue test data. Of interest in this study are the microstructures and welding defects produced by different welding processes. The microstructure of the welds affects the static properties, such as tensile strength and ductility, and the crack initiation and crack growth under cyclic loading. Defect size and location are two important parameters for damage-tolerant design. Based on the initial defect size, the fatigue life can be predicted and this concept is also used as baseline for setting up periodic inspection of components. Several factors are believed to contribute to fatigue crack initiation from a pore, such as stress concentration around a defect, its size and location, whether it is located near the surface, presence of other pores nearby, and residual stresses from the welding process. It is also believed that a critical size exists and that the presence of defects below this size does not affect the fatigue strength.

Welds produced with electron beam welding (EBW), laser beam welding (LBW), tungsten inert gas welding (TIG) and plasma arc welding (PAW) have different microstructures and different populations of defects in terms of their size and distribution. The effect of these aspects on mechanical properties under different testing conditions have been investigated in the present work.

## 1.1 Objective

The objective of the ongoing work is to study

- What kind of microstructures are produced with different welding processes and alloy compositions?
- What kind of defects exist for the different processes?
- How do different microstructures affect the mechanical properties?
- What size and distribution of defects affect the mechanical properties?

## 2 Background

### 2.1 Titanium industry and applications

Titanium alloys have appealing properties which is why they have found applications in a variety of fields. The biocompatibility of titanium makes it attractive for medical industry, resistance to corrosion makes it appealing for petrochemical and marine applications. Aerospace industry is one of the largest users of titanium alloys where they are used as material for fan and compressor structures in jet engines, airframe structures and landing gear in aircrafts, space rockets and satellites. The main reason for the large use of titanium alloys in aerospace industry is their excellent strength-to-weight ratio. Figure 1.1 shows a comparison of specific strength against temperature for several materials. Titanium alloys have the higher specific strength than most metals in temperatures below 400-500°C [1].

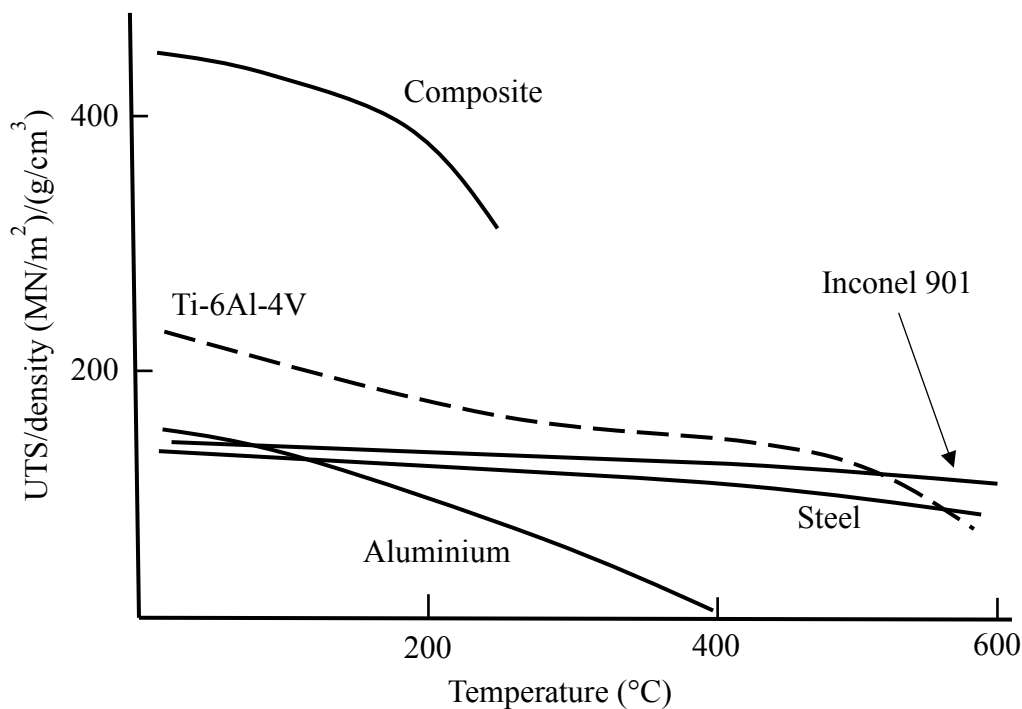


Figure 1.1. A comparison of specific tensile strength against temperature for various materials. Adapted from [2].

The primary factor limiting more extensive use of titanium is its cost. With a significantly higher cost than aluminum and steel alloys, titanium utilization must be justified for each application. The total cost of titanium stems from high extraction cost from ore to metal as well as high processing costs. Aluminium

sheet has the same cost as titanium sponge which needs several processing steps to achieve the finished product [3]. Also machining of titanium alloys is 10-100 times slower than aluminium alloys [1].

With these factors in mind, much research and development is being devoted to a reduction of the buy-to-fly ratio of titanium components. The buy-to-fly ratio refers to the weight ratio between the raw material and the weight of the final (flying) component after processing and manufacturing. Currently, in production of aerospace components nearly 90% of the original casting or forging weight can be machined away and turned into scrap. Reduction of the buy-to-fly ratio means that a reduced weight of a very expensive material is used and also reducing the amount of machining required to achieve the final product. Several technologies are being pursued to accomplish this. These include welding, greater use of extrusions where appropriate, superplastic forming and superplastic forming with diffusion bonding, hot stretch forming to obtain more precise formed shapes, as well as powder metallurgy and additive manufacturing [1].

## 2.2 Common titanium alloys and physical metallurgy

At room temperature, pure titanium has a hexagonal close packed (hcp) crystal structure which is referred as alpha ( $\alpha$ ) phase. At temperatures above 888°C, the structure transforms to a body centered cubic (bcc) crystal structure, called beta ( $\beta$ ) phase.

Alloying elements of titanium can be i)  $\alpha$  stabilizers which increase the  $\beta$  transus temperature, ii)  $\beta$  stabilizers which lower  $\beta$  transus temperature, or iii) act as solid solution strengtheners and do not affect the transition temperature.

The substitutional element Al and the interstitial elements O, N and C are strong  $\alpha$  stabilizers. V, Mo, Nb, Ta, Fe, Mn, Cr, Ni, Co, Cu and H are  $\beta$  stabilizing elements. Zr and Sn are neutral alloying elements which do not change the  $\beta$  transformation temperature. The increase in amount of  $\alpha$  stabilizers O, N and C leads to a significant increase in strength but at the same time to a sharp drop in ductility. Titanium has high chemical affinity to these elements especially at elevated temperature which is why inert atmosphere needs to be used when processing titanium at high temperatures [4], [5].

Titanium alloys are divided into three main groups,  $\alpha$ ,  $\alpha+\beta$  and  $\beta$  alloys, depending on which phases dominate at room temperature.

Commercially pure (CP) titanium alloys and  $\alpha$  alloys have hcp crystal structure at room temperature. They are insensitive to heat treatments and have good weldability. CP alloys possess the lowest strength but they exhibit the best corrosion resistance and have the best weldability. Oxygen and nitrogen are used as alloying

elements to increase the strength of CP alloys.  $\alpha$  alloys are slightly less corrosion resistant but higher in strength than unalloyed titanium.  $\alpha$  alloys cannot be strengthened by heat treatment because they are single phase alloys. The principal alloying element in  $\alpha$  alloys is aluminum but certain  $\alpha$  alloys contain small amounts of  $\beta$  stabilizing elements. Some of these alloys are called near- $\alpha$  alloys and can be heat treated to some degree.  $\alpha$  and near- $\alpha$  alloys are characterized also by their high creep resistance which is why they are preferred for use in high-temperature applications [4], [5].

$\alpha+\beta$  alloys contain both  $\alpha$  and  $\beta$  stabilizing elements and they are characterized by a superior combination of strength and formability. The microstructure and mechanical properties of  $\alpha+\beta$  alloys can be modified by adjusting the thermo-mechanical processing parameters [4], [5].

A  $\beta$  alloy is defined as a titanium alloy with sufficient  $\beta$  stabilizer content to suppress the martensitic transformation during quenching to room temperature.  $\beta$  alloys are metastable, and precipitation of  $\alpha$  phase and other phases from the metastable  $\beta$  is a method used to strengthen the alloys.  $\beta$  titanium alloys are the most versatile class of titanium alloys. They offer the highest strength to weight ratios and very attractive combinations of strength, toughness, and fatigue resistance. Some of the disadvantages compared to  $\alpha+\beta$  alloys are increased density, a rather small processing window, higher cost, and microstructural instability [4], [6].

### 2.2.1 Ti-6Al-4V alloy

Ti-6Al-4V (Ti-64) is one of the most important titanium alloys. It accounts for about 45% of the total weight of all titanium alloys produced and more than 80% of titanium alloys used in aerospace industry. Ti-64 is also used in medical implants and in automotive, marine and chemical industries. Ti-64 is an  $\alpha+\beta$  alloy which combines attractive mechanical properties with good workability and the best weldability of  $\alpha+\beta$  alloys. Application of Ti-64 is limited to about 350°C which limits its use in high temperature applications. In the aerospace industry, Ti-64 is extensively used in the cold section of jet engines, i.e. in the fan and compressor sections [4].

### 2.2.2 Boron modified Ti-alloys

Small boron additions to titanium alloys refines the solidification microstructure and  $\alpha$ -colony size dramatically. These microstructural refinements improve mechanical properties such as yield strength, ultimate tensile strength, tensile ductility, creep and fatigue behaviour [7]–[11]. However, addition of higher

amount of boron ( $> 0.1$  wt% B) increases the volume fraction of TiB particles, which in turn act as crack initiation sites during fatigue loading, and thus can reduce the overall ductility of the alloy [11], [12].

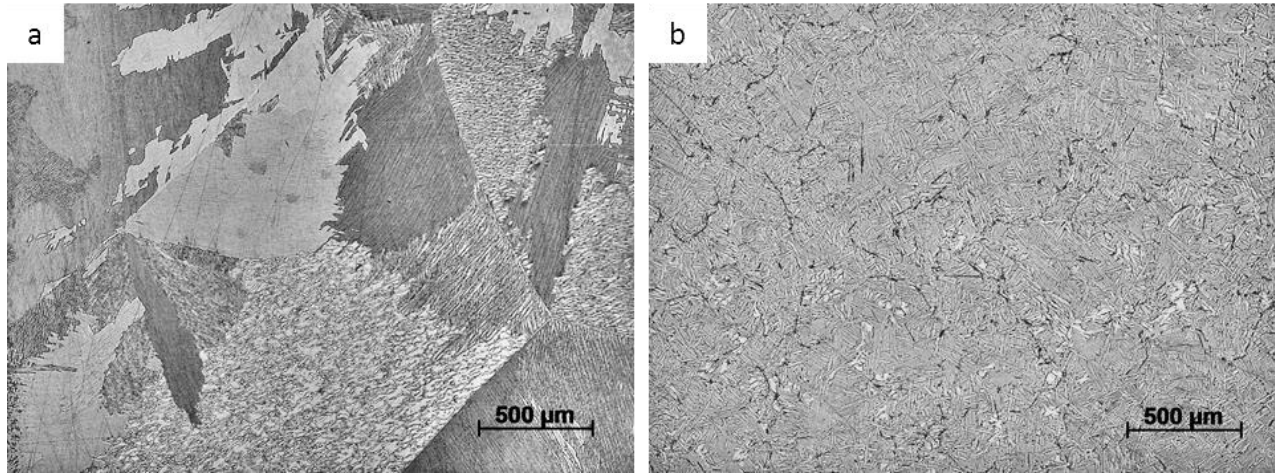


Figure 1.2. Effect of boron on microstructure of cast Ti-64: a) 0 wt-% B and b) 0,11 wt-% B.

Figure 1.2 shows the microstructure of cast boron modified Ti-64 alloy in comparison to an unmodified alloy. As can be seen the prior  $\beta$  grain size in cast Ti-64 is refined by an order of magnitude by trace addition of boron [7], [11]. Dark areas in prior  $\beta$  grain boundaries of the boron modified alloy are TiB particles which form via a eutectic reaction in the final stage of solidification. TiB particles also eliminate the grain boundary  $\alpha$  layer and refine the  $\alpha$  microstructure by acting as nucleation sites for new  $\alpha$  plates [10].

The mechanism of how boron refines the prior  $\beta$  grain size is related to its very low solubility in titanium. This causes boron to segregate strongly during solidification which develops a constitutionally super-cooled zone which restricts the growth of solid grains and allows other nucleation sites to activate and seed new grains [13].



### 3 Welding of titanium alloys

For successful welding of titanium, some factors need to be considered. Titanium is extremely reactive in temperatures exceeding 500-650°C. It reacts with elements in impurities or air such as C, O, N, and H. These elements strengthen titanium but small amounts also impair ductility and toughness of titanium joints. The effects of the heating and cooling cycles involved in welding processes on the mechanical properties of the alloys and the specific alloy composition also need to be considered [4].

#### 3.1 Welding processes

Titanium alloys are readily joined with several common fusion welding processes such as tungsten inert gas welding (TIG), plasma arc welding (PAW), electron beam welding (EBW), and laser beam welding (LBW). Fusion welding processes can be characterized generally by the heat-source intensity. Figure 3.1 illustrates the different characteristics of the aforementioned welding processes and how they affect the penetration.

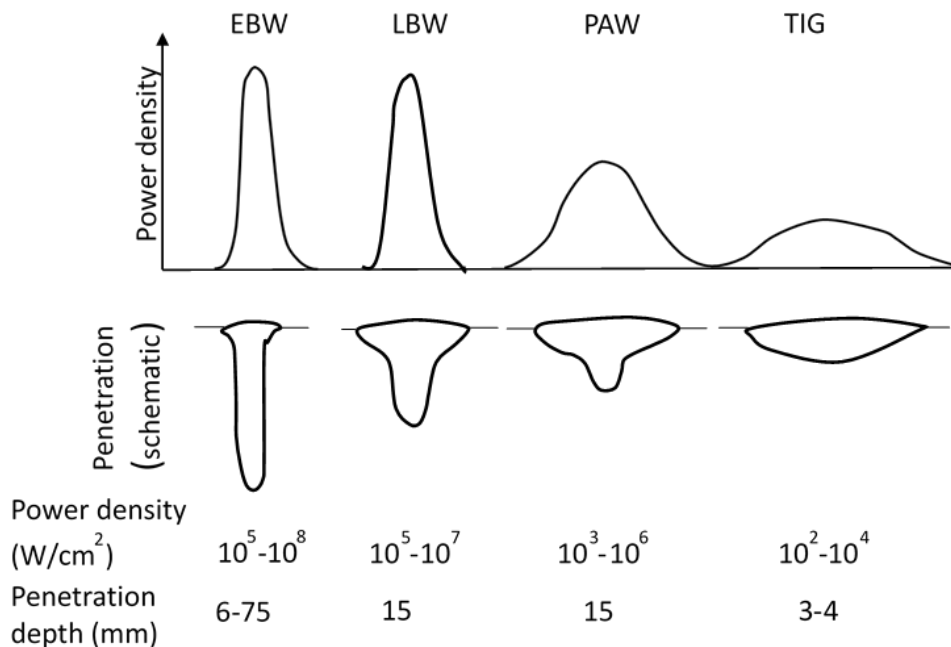


Figure 3.1. Spectrum of practical heat intensities used for fusion welding. Adapted from [14], [15].

The major advantage of high energy beam welding techniques is the ability to produce welds that are deeper and narrower than by arc welding. Also a much lower heat input is used than what is required in arc welding. The lower heat input results in a narrow fusion zone and heat affected zone and noticeably smaller thermal effects on the workpiece leading to smaller residual stresses and distortions.

### 3.1.1 Tungsten inert gas welding

Tungsten inert gas welding (TIG) or gas tungsten arc welding (GTAW) refers to an arc welding process using an arc between a non-consumable tungsten electrode and the workpiece. The electric arc is produced by the passing of current through conductive ionized shielding gas. Shielding gas is fed through the torch to provide an inert atmosphere that protects the electrode and the weld pool while the weld metal is solidifying. Argon, helium and their mixtures are used as shielding gases. TIG can be used to produce welds autogenously or a filler material, usually a wire, can be added to the weld pool to fill the joint. The TIG welding process is illustrated in Fig. 3.2.

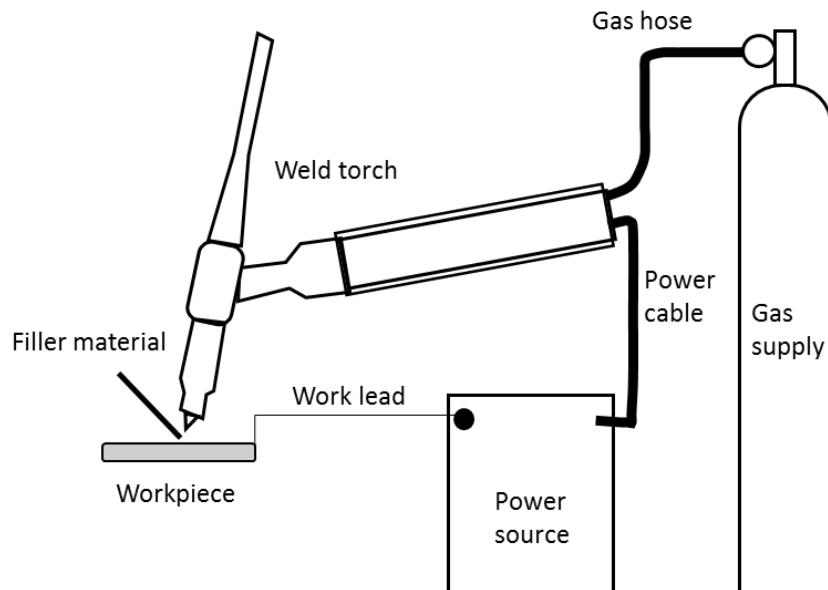


Figure 3.2. Schematic illustration of typical TIG equipment. Adapted from [14].

TIG is a flexible process that can be used to produce high quality welds in many otherwise difficult to weld metals such as magnesium, aluminium, titanium, stainless steels and nickel-based superalloys. TIG is best suited for welding relatively thin sections up to approximately 9.5 mm [14]. TIG can be used manually or automated. The heat source and filler metal additions can be controlled independently. The process can be

used with or without filler metal. Welds are generally high quality, spatter-free, include few defects and there is no slag, hence no post weld cleaning is required. A further advantage is the relatively low cost of the equipment.

The limitations of TIG include the relatively low welding speed and deposition rate which makes it inefficient to weld thick sections. TIG has low tolerance for contaminants in filler and base material and magnetic fields leading to deflection of the arc can make the process difficult to control. Also the heat input of TIG process is relatively high.

The main process parameters in TIG welding are arc voltage, welding current, travel speed, wire feed and shielding gas. The amount of energy produced by the arc is proportional to the current and voltage. The amount of energy transferred per unit length is inversely proportional to the travel speed. Helium as a shielding gas produces a hotter arc and deeper penetration than argon. An alternating welding current can be used for better oxide removal and improving welding characteristics. Pulsing of the welding current can be used to control heat input and increase penetration [14], [16].

### 3.1.2 Plasma arc welding

Plasma arc welding (PAW) is an arc welding process which uses a constricted arc between a non-consumable electrode and the workpiece (transferred arc mode) or between the electrode and the nozzle (nontransferred arc mode). Two separate gas flows are used in PAW; plasma gas which flows through the orifice and becomes ionized and shielding gas which flows through the outer nozzle. Usually these gases are the same. Helium, argon and their mixtures are used as shielding gases. Hydrogen and nitrogen may also be added in the mixture. PAW is essentially an extension of the TIG welding process and the differences between the processes are illustrated in Fig. 3.3. TIG uses an open arc while in PAW, the electrode and arc are surrounded by a gas chamber. The plasma gas in the orifice gets heated and ionized which creates a narrow, constricted arc that provides excellent directional control and produces a very favorable depth-to-width weld profile.

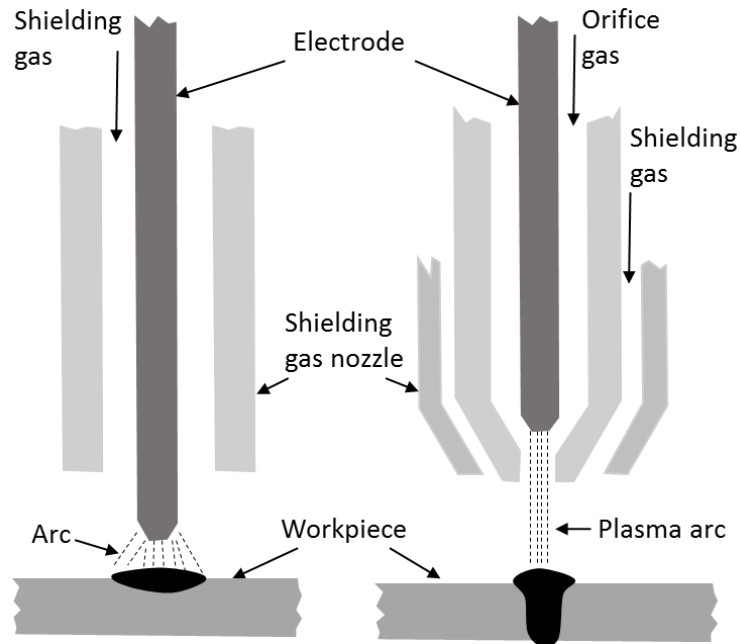


Figure 3.3. The plasma arc is confined in PAW which makes it straighter and more concentrated. Adapted from [16].

PAW can be used in two distinct operating modes, the melt-in mode and the keyhole mode. At lower arc currents, the process resembles TIG and produces a similar weld pool. This melt-in mode is used for material thicknesses below 3 mm. At higher arc currents and plasma gas flow rate, the plasma column can displace the molten metal and form a keyhole. Keyhole mode welding is used for single pass butt welds on material thicknesses from 2.4 mm to 8 mm. Compared to laser welding and electron beam welding, keyhole PAW is more cost effective and more tolerant of joint preparation, though its energy is less dense and its keyhole is wider [17].

The advantages of PAW compared to TIG include:

- High welding speed: up to 5 times higher than conventional TIG
- Reliable arc ignition and concentrated stable arc with little sensitivity to arc length variation
- Lower heat input leading to smaller heat affected zone and little distortion
- Ability to perform keyhole welding and melt-in-mode welding with the same equipment
- Possibility to weld very thin materials (0.1 mm) and thick materials (8 mm) with a single pass without filler material
- High metallurgical quality in comparison to conventional TIG.

PAW can be used to weld the same materials as TIG. Keyhole plasma welding is extensively used to weld stainless steel pipes and tanks. In aerospace industry, PAW is used for airframe components, fuel vessels and gas turbine components. The greater capital cost and complexity of PAW equipment are why PAW has not become more common [16].

### 3.1.3 Laser beam welding

Laser beam welding (LBW) uses a concentrated laser beam as the source of heat. The coherent nature of the laser beam allows it to be focused to a small spot which allows narrow and deep welds with high welding rates.

The first laser was introduced in 1960 but its use for welding application was limited until the introduction of high-power continuous-wave lasers in the 1970s. High-power continuous-wave lasers include CO<sub>2</sub>, Nd:YAG, fiber, disk and most recently high-power diode lasers. A comparison of properties between different types of lasers is shown in table 3.1.

Table 3.1. Properties of high-power lasers [15].

	Wavelength [ $\mu\text{m}$ ]	Average continuous power [kW]	Beam quality
CO <sub>2</sub>	10.6	50 max, 1-15 normal	Average-Good
Nd:YAG	1.06	10 – 15	Poor
Fiber	1.07	100	Good
Disk	1.03	16	Good
Diode	0.98	10-15	Poor

CO<sub>2</sub> lasers were the first high-power lasers used for welding applications. Until recently CO<sub>2</sub> lasers have offered the highest output power, good beam quality and relatively low machine cost making them an attractive alternative especially for welding thick sections. CO<sub>2</sub> lasers operate at 10.6  $\mu\text{m}$  wavelength which causes most of the disadvantages related to CO<sub>2</sub> lasers. Common transparent materials such as glass and quartz are opaque to 10.6  $\mu\text{m}$  wavelength laser radiation which makes it impossible to use optical fiber systems. This limits the flexibility of CO<sub>2</sub> laser systems. 10.6  $\mu\text{m}$  wavelength has also lower absorptivity on metals and higher absorptivity on laser induced plasma [15].

Solid state lasers operating at wavelengths close to 1  $\mu\text{m}$  have a benefit that the laser radiation can be delivered via optical fiber which makes the laser systems more flexible. 1  $\mu\text{m}$  radiation has higher absorptivity on metals and lower absorptivity on the plasma. Early high-power solid state lasers, Nd:YAG lasers, had relatively poor beam quality and electrical efficiency. The development of disk and fiber lasers has improved the beam quality and electrical efficiency significantly. Direct diode lasers are the latest development. They have excellent electrical efficiency and compact size but poor beam quality allows only conduction mode welding [15].

Laser beam welding has numerous benefits over traditional welding methods. However, it has also several limitations that need to be considered.

Major advantages of LBW include:

- Focused laser light provides high energy density
- High processing speed and narrow welds with deep penetration
- Heat input is close to the minimum required to fuse weld metal. Distortions and metallurgical effects in heat affected zone are minimized
- Can be used under ambient atmosphere or shielding gas. No vacuum required
- No electrodes or filler materials required
- Difficult-to-weld materials, such as titanium and quartz, can be joined
- Can be used in keyhole mode or conduction mode
- Can be readily mechanized for automated high-speed welding
- The laser beam can be transmitted to several workstations using beam-switching optics

Limitations of LBW include:

- Laser welding equipment is almost 10 times more expensive than comparable arc welding system although they are cheaper than EBW systems and have higher productivity than conventional arc welding
- Joints must be accurately positioned because of small size of the laser beam
- Maximum joint thickness is limited compared to EBW
- The high reflectivity and high thermal conductivity can affect laser weldability of some materials [14], [15], [18].

### 3.1.4 Electron beam welding

Electron beam welding (EBW) is a high energy beam welding process, which uses a focused beam of electrons to melt the workpiece surfaces and create the joint. A high intensity beam of high velocity electrons

are concentrated onto a small area. Power densities as high as  $10^8$  W/cm<sup>2</sup> can be achieved. The high power density can lead to keyhole formation which distinguishes EBW and other high energy density processes from other welding methods.

EBW has the following characteristics in comparison to other weld methods:

- High power density of about  $10^8$  W/cm<sup>2</sup> with a focused beam. A comparison to other welding processes is shown in Fig. 3.1
- High welding speed which results in welds with high depth-to-width ratio, small heat affected zones and little distortion.
- Production of welds with very shallow to very deep penetrations. More than 250 mm have been reported.
- The welding process is commonly carried out in vacuum which provides good protection of the weld pool against contamination.

The capital cost of EBW equipment is a major drawback in comparison to conventional welding processes. The cost of joint preparation and tooling is also higher because the small electron beam spot size requires precise joint gap. The vacuum chamber limits the size of the workpiece and the production rate is affected by the need to evacuate the chamber for each production batch [14], [18].

## 3.2 Welding metallurgy of Ti-6Al-4V

### 3.2.1 Solidification

Ti-64 has very narrow freezing range, approximately 5°C, hence, it behaves like a pure metal during solidification. The narrow freezing range and absence of segregating elements and low melting phases makes Ti-64 welds unsusceptible to solidification related cracking which may be a problem for other high strength structural metals [4].

During solidification,  $\beta$  grains nucleate epitaxially and grow preferentially towards the maximum heat gradient. The favoured growth direction for the dendrites in bcc metals is in the  $\langle 100 \rangle$  direction. Therefore the nucleation sites with the  $\langle 100 \rangle$  direction aligned with the temperature gradient will outgrow less favourably oriented grains. Large grains in the base material and in the heat affected zone provide fewer epitaxial growth sites at the fusion boundary and dictate large prior  $\beta$  grains in the fusion zone [19]. Large grains in the base material and the heat affected zone provide fewer epitaxial growth sites at the fusion boundary and dictate large prior  $\beta$  grains in the fusion zone [19]. Under two-dimensional heat flow conditions, which is typical for keyhole EBW and LBW, columnar  $\beta$  grains growing from base material

inwards are formed. Under three-dimensional heat flow conditions, typical for TIG, more complex, multidirectional  $\beta$  grain morphologies are formed [4]. Prior  $\beta$  grain size in the weld zones increases with increasing heat input of the welding process [19], [20].

### 3.2.2 Continuous cooling

$\alpha+\beta$  titanium alloys such as Ti-64 form complex microstructures during continuous cooling from  $\beta$  phase field. Depending on the cooling rate from  $\beta$  phase field, the transformation can be diffusionless (martensitic) or nucleation and diffusion controlled. For high cooling rates the transformation will be diffusionless forming martensite. In titanium alloys two martensite morphologies are observed, massive and acicular martensite. The massive martensite consists of very thin laths (0.1-1  $\mu\text{m}$ ), which all have similar crystal orientation and can be observed as irregular areas that are hard to resolve with light optical microscope. The acicular martensite consists of individual  $\alpha$  laths, each with different crystal orientation [5].

Slower cooling rates lead to a diffusion controlled transformation. The  $\alpha$  phase first nucleates preferentially at  $\beta$  grain boundaries forming a continuous  $\alpha$  layer along  $\beta$  grain boundaries. During continued cooling,  $\alpha$  plates nucleate at the  $\beta$  grain boundaries and grow into the  $\beta$  grains as parallel plates belonging to the same variant of the Burgers relationship forming so-called  $\alpha$  colony. The  $\alpha$  colonies continue to grow until they meet another  $\alpha$  colony. With increasing cooling rate, the size of the  $\alpha$  colonies as well as the thickness of the individual  $\alpha$  plates becomes smaller. At higher cooling rates  $\alpha$  plates start to nucleate also at the  $\alpha$  colony boundaries and start to grow perpendicular to the nucleation site forming basketweave structure [5].

Ahmed and Rack [21] demonstrated that martensitic, massive and diffusion controlled phase transformations occur in Ti-64. Cooling rates above 410 $^{\circ}\text{C}/\text{s}$  are required to achieve fully martensitic microstructure, a massive transformation is observed between 410 and 20 $^{\circ}\text{C}$  which is gradually replaced by diffusion controlled Widmanstätten  $\alpha$ -formation. The microstructure formed through diffusional transformation is also influenced by the cooling rate. Faster cooling rates promote formation of basketweave microstructure, while lower cooling rates favor formation of larger  $\alpha$  colonies [22]. The grain boundary  $\alpha$  layer in prior  $\beta$  grain boundaries forms diffusionally and is typically observed in cast and weld materials with lower cooling rate [5].

High energy beam welding processes such as EBW and LBW can have cooling rates between 100 to 1000  $^{\circ}\text{C}/\text{s}$ . Microstructures produced by these processes can be entirely martensitic. For arc welding processes such as TIG and PAW cooling rates between 10 to 150  $^{\circ}\text{C}/\text{s}$  have been reported, which can produce a microstructure with a combination of martensitic  $\alpha'$ , massive  $\alpha_m$  and diffusional  $\alpha$  [23].



### 3.2.3 Post weld heat treatment

Post weld heat treatments are applied on welds to relieve residual stresses, stabilize and homogenize the weld zone microstructure and to improve ductility [23]. Microstructural changes occur during post weld heat treatments. In Ti-64, it has been observed that martensitic  $\alpha'$  decomposes to equilibrium  $\alpha$  and  $\beta$ . Martensite decomposition is not completed at temperatures below 600°C. A temperature of 700-800°C is required for complete decomposition of martensite [24]. The microstructure coarsens during post weld heat treatment. At temperatures below 700°C no significant coarsening occurs whereas at temperatures 800-900°C coarsening has been observed [25]–[27]. The ductility improves with increasing post weld heat treatment temperature but cannot be fully restored in  $\alpha+\beta$  titanium alloys. Fracture toughness is also improved with increasing temperature [23].

## 3.3 Typical defects in titanium alloy welds

### 3.3.1 Cracking and embrittlement

Compared to other alloys, such as nickel based super alloys and stainless steels, titanium alloys are not considered susceptible for solidification related cracking because of low concentration of impurities. Titanium alloys have been reported to crack if welded under severe restraint [28] but the Ti-64 alloy has excellent cracking resistance. The absence of precipitate particles, impurities at grain boundaries and low melting temperature phases in most titanium alloys makes them very resistant to HAZ or liquation cracking [4].

Contamination cracking is a problem for titanium alloys. If titanium is exposed to air, moisture or hydrocarbons at temperatures exceeding 500°C, the material will absorb oxygen, nitrogen, carbon and hydrogen. These interstitial elements inhibit plastic deformation and increase strength but cause a decrease of ductility. Iron or tungsten particles are also reported to cause embrittlement. If the contamination level exceeds a certain amount, residual stresses generated by welding can cause cracking. At increased oxygen contents weld bead discoloration can occur as well as an increase in the surface hardness of the weld [4].

Contamination cracking can be avoided by protecting the heated weld region from interstitial elements. High purity inert welding gas needs to be used to shield the weld pool, trailing shield and the backside of the joint. Thorough cleaning and degreasing of joint surfaces is required [4].

### 3.3.2 Porosity

Porosity is a concern for high performance components that are subjected to cyclic loading as pores reduce the fatigue resistance of the welds. Several studies indicate a significant decrease in fatigue life of welds containing porosity compared with defect-free welds [29]–[31]. Surface porosity has shown to be especially detrimental. Porosity is a concern particularly in components where the weld profiles are dressed or machined away. In such components the geometrical defects in the weld profile do not affect fatigue life and internal pores can break a surface, and act as stress concentrators [32].

There are many reasons for porosity formation in welding such as shrinkage of the weld material, trapping of shielding gas, chemical reaction in the welding pool, keyhole instabilities, and evaporation [33]–[36]. The pores are often classified based on their shapes; rounded pores are classified as gas pores, irregular pores are classified as shrinkage pores. In titanium alloy welds spherical gas pores are the most prevalent [34].

Weld metal porosity is reported to form easily in keyhole laser welding. Several studies have shown that keyhole instability can lead to metal vapor or inert gas getting trapped in the weld metal [37], [38]. This occurs when the forces keeping the keyhole open are not in balance with the forces that try to close the keyhole. The attenuation of laser radiation by plasma or vapor has been recognized as a reason for keyhole fluctuation. Other effects such as localized evaporation may cause a large dynamic pressure that may cause keyhole instability generating porosity [36]. Relatively large pores can form this way. Modulation of laser power has been shown to decrease the porosity in keyhole laser welding as well as using directed gas jets or dual focus lasers to stabilize keyhole [39]. High beam quality fiber and disk lasers have been shown to produce welds with reduced porosity in comparison to Nd:YAG lasers [39]. Vacuum welding has been effective in the prevention of porosity and also penetration depth has increased [40]. Conduction mode laser welding is a more stable process and has been reported to produce welds free from porosity [39]. Keyhole plasma welding has been reported to produce welds with very little porosity in comparison to other fusion welding processes [29].

Hydrogen is recognized as another major cause for porosity in titanium alloy welds. The hydrogen solubility in titanium increases as the temperature decreases. There is a sharp decrease in solubility at the solidification point, which causes the rejection of small hydrogen bubbles in the melt pool as the weld solidifies. Typically, a hydrogen content of 210 ml/100 g is required for hydrogen bubbles to be rejected, which is much more than the hydrogen content in modern titanium alloys. There are other potential sources for hydrogen such as:

- preparation of joint surface,
- welding consumables,
- shielding gas, and
- the hygroscopic titanium oxide layer.

Workpiece preparation is essential in avoiding hydrogen porosity. Removal of the hydrated oxide layer and other surface contaminants is important in minimizing the hydrogen content in the melt pool. Mechanical cleaning and chemical pickling with a solution of hydrofluoric acid and nitric acid has been shown to be effective [29], [34]. The time between joint preparation and welding should be minimized, because the oxide layer continues to absorb moisture [34], [35]. The surface roughness can be a factor as small cavities at the surface can act as nucleus for pores [41]. Other sources of hydrogen may be the shielding gas or the filler material which is why high-purity shielding gases and extra low interstitial filler materials are used [34].

Hydrogen induced porosity has been reported to occur in various processes. In EBW it has been suggested to be the main reason for porosity [35], [41]. In LBW two types of porosity have been reported. Process induced pores are typically larger and hydrogen porosity smaller [36].

### 3.3.3 Geometrical weld profile defects

Geometrical weld profile defects can occur because of the welding process or due to the joint configuration. For example joint misalignment is not directly related to the welding process but occurs more commonly in keyhole laser or electron beam welding as the narrow beam can more easily miss the joint line. Incorrect clamping, restraint or inadequate machining may lead to other geometrical defects [34], [42]. Geometrical defects related to welding process include humping, undercut, slumping, concavity, lack of penetration, burn through and spatter. Usually it is possible to find a balance of process parameters, such as weld speed and power, to achieve required weld penetration and minimize weld-profile defects. For example humping is usually observed at high welding speeds [42]. In laser welding underfill depth has reported to decrease with increasing welding speed as less evaporation occurs [43].

Titanium has some favourable properties such as good weldpool fluidity, low thermal conductivity, low density and high surface tension. These characteristics are favourable in minimizing weld geometry defects and allow welding with an unsupported root surface [23].

Geometrical weld defects are particularly harmful in components subjected to dynamic loading. The defects at the surface of the components act as stress concentrators and initiate fatigue cracks. In some cases remelting the weld surface, i.e. dressing, or machining can be used to reshape the weld geometry and remove the geometrical defects [32].

### 3.4 Mechanical properties of Ti-6Al-4V welds

According to Lütjering [5] the critical microstructural parameters for fully lamellar microstructures with respect to mechanical properties are the  $\beta$  grain size, the  $\alpha$  colony size, the width of the  $\alpha$  plates and presence of grain boundary  $\alpha$  layer. The most critical parameter is the size of  $\alpha$  colonies which defines the effective slip length. Decreasing  $\alpha$  colony size improves the yield strength, the ductility, the micro crack nucleation and propagation resistance, whereas the macro crack propagation and fracture toughness are improved by large  $\alpha$  colony size. Large increase in the yield strength is observed when the colony structure changes to martensitic microstructure and slip length equal the width of individual  $\alpha$  plates.

Tensile ductility of fully lamellar microstructures is lower in comparison to the bi-modal microstructures. Microvoids can nucleate in the  $\alpha$ - $\beta$  interface and due to large aspect ratio of  $\alpha$  platelets there is a large amount of these interfaces in fully lamellar microstructures. Reducing prior  $\beta$  size has a positive effect on tensile ductility [5], [44]. If the strength difference between the intragranular microstructure and the grain boundary  $\alpha$  layer is great, the cracks can nucleate at the grain boundary  $\alpha$  layer causing less ductile intergranular fracture [5].

For welds this means that the fine lamellar microstructure formed in the fusion zone and heat affected zone has higher hardness than the base material. The ultimate tensile strengths of welds have been reported to be 925 MPa to 1060 MPa. Welds have been reported to have both higher and lower strengths than base material depending on the welding process and the post weld heat treatment [23]. The martensitic microstructures formed in high energy intensity processes have typically higher hardness and strength than welds produced by arc welding processes [25].

The tensile ductility of welds is lower in comparison to the base material. Tensile elongation as low as 6 % has been reported for the welds while 11 % (cast) to 16 % (wrought) elongation is typical for base material. TIG welds have the lowest ductility while EBW welds have been reported to have the highest [44]–[47]. Post weld heat treatments improve the ductility of the welds but not to the level of the base material [25], [48]. The ductility of welds can be also improved by reducing the prior  $\beta$  grain size. Using pulsed current in TIG welding resulted in welds with smaller prior  $\beta$  grain size and better ductility. The smaller prior  $\beta$

grain size in welds produced by EBW may explain their better ductility in comparison to TIG welds [20], [23], [44], [45].

Fracture toughness and resistance to fatigue crack growth is typically better in the welds than in the base material due to the fine lamellar microstructure [25], [49]. In defect free structures fatigue cracks occur in area of lowest strength which in weldments is located some distance from the base material [50]. In welds joint geometry, defects, and residual stresses can reduce the fatigue performance significantly [29].

## 4 Fatigue

Engineering components are frequently subjected to repeated loads, and the resulting cyclic stresses can lead to microscopic physical damage to the materials involved. This microscopic damage can accumulate with continued cyclic loading even at stresses well below material's ultimate strength. The microscopic damage can develop into a crack which can lead to failure of the component. This process of damage and failure due to cyclic loading is called fatigue [51].

The fatigue process is usually divided in three stages, the crack initiation, the crack growth and the final fracture as illustrated in Fig. 4.1.

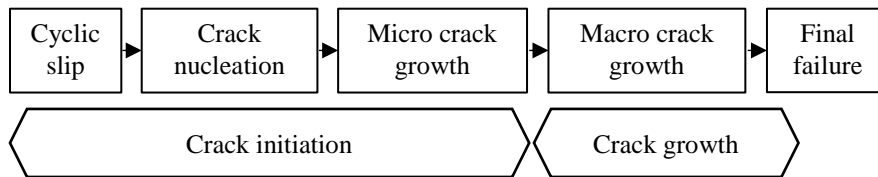


Figure 4.1. Schematic sketch of the different phases for the fatigue failure process. Adapted from [32].

Cracks often nucleate at the surface of the material due to cyclic slip occurring in the planes of maximum shear stress in favorably oriented grains. Micro cracks initiate along these slip lines. The nucleation rate of micro cracks depends to a large extent on the applied loading conditions. In general, with increasing load the number of cycles for fatigue crack initiation decrease. In spite of early crack nucleation, the growth of micro cracks is slow and they remain invisible for a considerable part of the total fatigue life. Once cracks become visible, the remaining fatigue life of a laboratory specimen is usually a small percentage of the total life. The growth of micro cracks is affected by crack growth barriers such as grain boundaries which makes the small crack growth rate irregular or retard the crack growth and turning it into a non-propagating micro crack. Non-propagating cracks can initiate at stresses lower than the fatigue limit [32], [52].

The crack initiation phase is supposed to be completed when micro crack growth is no longer depending on the material surface conditions but the bulk properties of the material are controlling the crack growth rate. The size of the micro crack at the transition to the crack growth depends on microstructural barriers to be overcome and can significantly differ for different materials. Usually, the crack is growing perpendicular to the main principal stress. The final fracture will take place when the crack becomes so large that the

remaining part of the cross section is too small to withstand the load and subsequently complete fracture happens [32].

Cracks nucleate at the free surface because of reduced constraint for slip from adjacent grains, notch effects of surface imperfections and effects of surrounding environment. Cracks can also initiate at grain boundaries or internal inclusions and defects. These defects are normally not considered to be harmful for static strength but could affect the stress distribution on a microlevel and thus contribute to crack nucleation [32].

## 4.1 Fatigue in welds

Welding is used in a large portion of many engineering structures and it provides numerous structural design options which cannot be realized with other production techniques. However, the fatigue strength of welded structures is normally lower than that of unwelded components. This is also illustrated in Fig. 4.3 which shows a schematic sketch of the stress-life curves of a i) smooth plate, ii) a plate with a hole, and iii) a fillet weld [53].

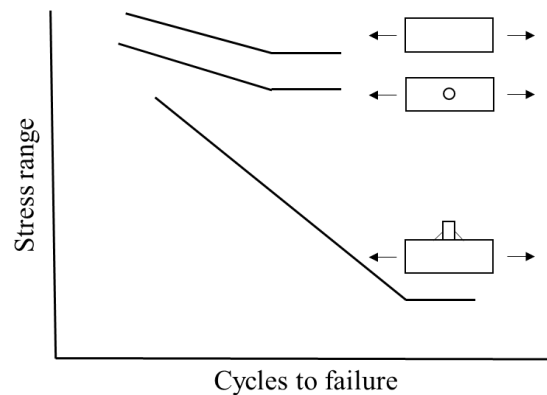


Figure 4.2. Fatigue strength comparison between a smooth plate, a plate with a hole and a fillet weld. Adapted from [53].

Fatigue strength of welded structures is problematic due to many factors intrinsic to welded joints. The welding process introduces changes to the material that can lead to reduction in fatigue strength. The main factors include stress concentration due to weld geometry, tensile residual stresses and presence of weld defects.

A weld profile causes a change in shape and hence will result in stress concentration. This stress concentration occurs at the toe of the weld that is the junction between the base material and the weld metal. The magnitude of the stress concentration depends on how sharp the geometrical change in the weld profile is. The weld toe is a common site for fatigue cracking in welded joints loaded transverse to the joint [53].

Residual stresses are formed during welding when the weld metal cools down and contracts. This causes tensile residual stresses to form in the weld, compressive residual stresses further away and distortions of the welded structure. The tensile residual stresses can approach the yield strength of the base material which contributes significantly to a reduction of fatigue strength in welded structures [53].

Welding defects such as slag inclusions, gas pores, lack of penetration at the weld root, and undercut at weld toes may be present in welded joints. Typical defects in titanium alloy welds are discussed in paragraph 3.3 and the effect of defects on fatigue strength is discussed more in paragraph 4.3.

## 4.2 Stress based method for fatigue analysis

There are three major approaches for analysis and design with respect to fatigue: i) stress based approach, ii) strain based approach, and iii) fracture mechanics approach. Since in this project all the fatigue tests have been performed with a stress control approach, the main concepts of this method will be discussed in more detail.

A cyclic loading between maximum stress,  $S_{max}$ , and minimum stress,  $S_{min}$ , can be characterized by the following values: stress range ( $\Delta S$ ), stress ratio ( $R$ ), and mean stress  $S_m$ .

$$\Delta S = S_{max} - S_{min} \quad (1)$$

$$R = \frac{S_{min}}{S_{max}} \quad (2)$$

$$S_m = (S_{max} + S_{min})/2 \quad (3)$$

Material testing for this approach is done in load-controlled method, testing the material at different stress levels. The results of such a test may be plotted to obtain a stress-life curve, or S-N curve. When the fatigue life,  $N_f$  is plotted against stress range in a log-log plot with sufficient number of data points, a straight line can be fitted to the data. Such a curve is called S-N curve and the corresponding equation will be of the form:



$$\Delta S = AN_f^B \quad (4)$$

where A and B are fitting constants.

Figure 4.2 shows typical S-N curves. S-N curves vary with material, its processing, stress ratio, chemical and thermal environment, frequency of loading and residual stress. Some materials like low alloy steels and titanium alloys exhibit a fatigue limit or endurance limit, a stress range below which fatigue failure does not occur and life is infinite. For other materials such as aluminum, that do not have a fatigue limit, fatigue strength is defined as stress range at a specific life.

The stress based approach provides a good approximation at low stress levels when the loading causes only elastic strains. This regime is called high cycle fatigue (HCF). If plastic strains are involved the life is shorter and this method fails to model fatigue behavior accurately. The regime of low cycle fatigue (LCF) is better approximated using strain based approach. The regime where high-cycle fatigue starts varies with material, but is typically from  $10^4$  cycles upwards [51], [53].

The fracture mechanics approach is a technique based on the analysis of fatigue crack growth. It takes into account the pre-existing defects in the material. The pre-existing defects can develop into cracks which can start growing. The fatigue material properties are characterized by the threshold stress intensity range,  $\Delta K_{th}$ , the fatigue crack growth rate relationship,  $da/dN$  vs.  $\Delta K$ , and the critical stress intensity factor,  $K_c$ , which corresponds to the fracture toughness of the material. The cyclic loading is described by stress intensity factor  $\Delta K$ , which depends on the stresses, geometry parameters and the size and shape of the crack [51].

### 4.3 Effect of weld metal porosity on fatigue

As described earlier, welding introduces imperfections to the welding joints which affect the fatigue performance. In situations where the external weld geometry is left intact, fatigue cracking can reliably be predicted to initiate from the weld toe. Even if geometry specific stress-raisers, such as weld toes, are removed in order to maximize the fatigue performance of the joints, fatigue strength can still be lowered significantly by the presence of weld metal porosity as shown in Fig. 4.3 [54], [55].

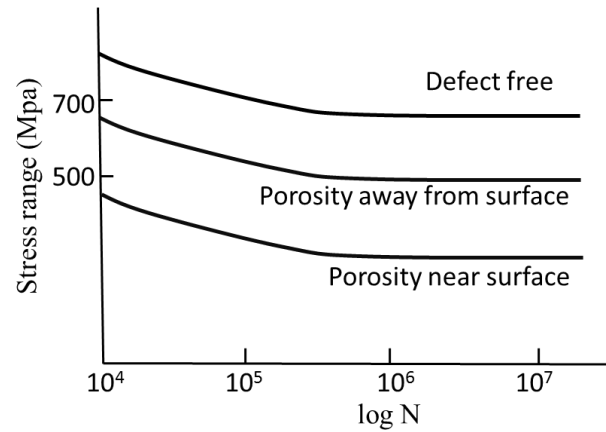


Figure 4.3. Comparison of fatigue data of Ti-64 welds with and without porosity. Adapted from [56].

The influence of defects and porosity on crack initiation and fatigue life has been examined by both experimental observations and theoretical modeling [57]–[62]. Pores have been found to initiate fatigue cracks in welds, in materials produced by additive manufacturing as well as in cast materials. Size and location of pores are important. It has been shown that pores close to or at the surface cause the highest stress concentration. Two adjacent pores cause an increased stress concentration if the distance between the pores is less than their diameters [57]–[59]. According to Murakami et al. [63], once a crack has initiated at a defect, the size of the crack determines the stress intensification at the crack tip. If the size of the crack is small enough, the stress intensification can be below the threshold value for crack growth and thus the crack can become a non-propagating crack.

## 5 Experimental techniques

### 5.1 Materials

In paper 1 and 3, Ti-64 sheet material (AMS4911) in annealed condition was used as parent material. The chemical compositions of used materials are shown in Table 5.1.

In paper 2, cast Ti-64 and Ti-64 with Boron additions were obtained from Titanium Castings Ltd, UK for this study. After casting, the ingots were hot isostatically pressed (HIP) at 900°C at 100 MPa for 2 hours.

For TIG welding Ti-64 welding wire was used. The chemical compositions of the three different alloys are shown in Table 5.1.

Table 5.1. Chemical compositions of materials used in experimental work.

Alloy	Al	V	Fe	O	C	N	H	Y	B	Ti
Ti64 sheet	6.12	3.81	0.17	0.12	0.006	0.005	<0.001	<0.005	-	Bal.
Ti64-0.00B	6.16	4.04	0.20	0.20	0.010	0.002	<0.001	<0.001	<0.001	Bal.
Ti64-0.06B	6.24	4.06	0.18	0.19	0.012	0.003	<0.001	<0.001	0.06	Bal.
Ti64-0.11B	6.18	4.02	0.19	0.24	0.07	0.004	<0.001	<0.001	0.11	Bal.

### 5.2 Welding

The welding experiments were performed at GKN Aerospace Engine Systems in Trollhättan, Sweden.

In paper 1 and 3 a 4 mm thick Ti-64 sheet material (AMS4911) was used as base material to produce welds with TIG, PAW, EBW, and LBW. The EBW, LBW and PAW were produced autogenously and for the TIG weld a filler wire was used. Standard welding parameters were used for these processes. Laser welded sheets are shown in Fig 5.1.

In paper 2 bead-on-plate TIG and LBW welds were produced on 8.5 mm thick sections of cast and HIPed conventional Ti-64 alloy and Ti-64 with 2 different boron concentrations. For TIG welding a partial penetration beads, and for laser beam welding full penetration beads, were obtained. Finished welds are shown in Fig 5.2.

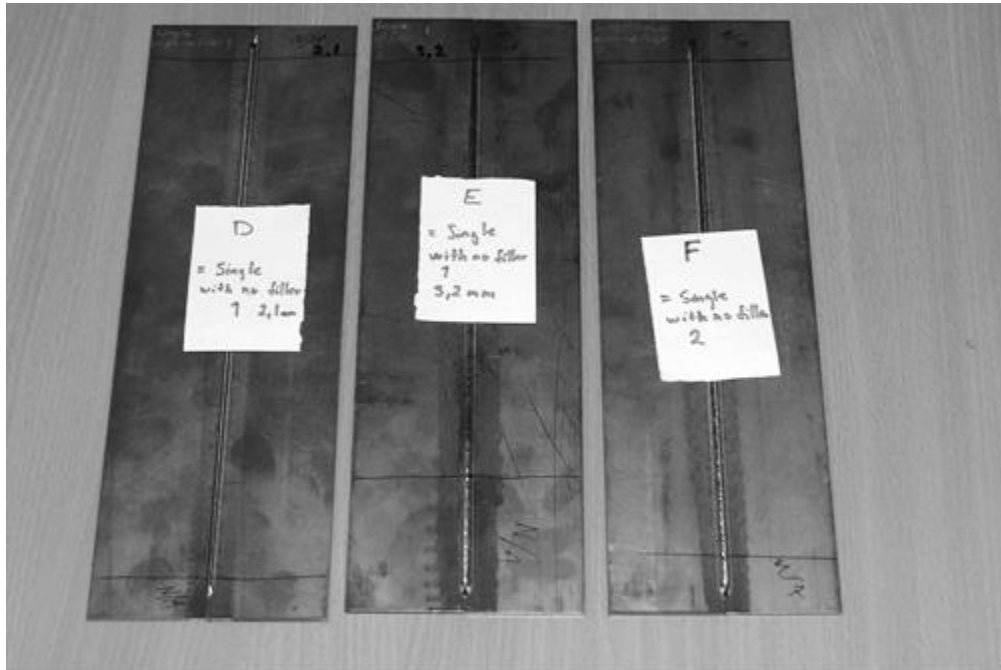


Figure 5.1. Laser beam welds on Ti-64 sheets used for mechanical testing.

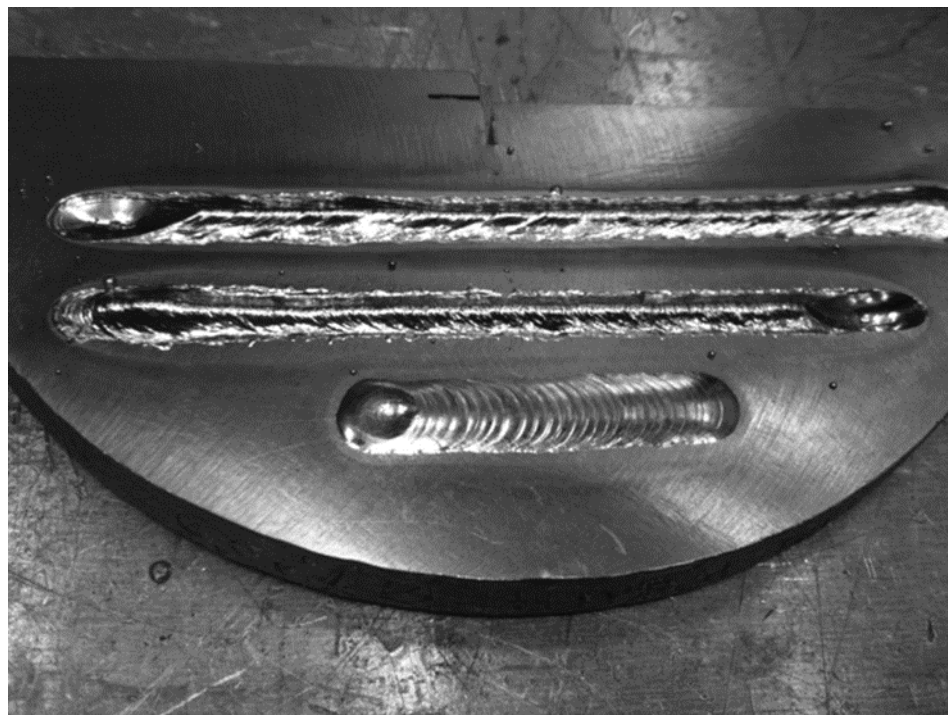


Figure 5.2. LBW welds (top) and a TIG weld (bottom) on cast and HIPed boron-alloyed Ti-64.

## 5.3 Microstructural characterization

### 5.3.1 Specimen preparation and optical microscopy

The specimen preparation for microstructural characterization was performed using conventional metallographic techniques used for titanium alloys. Careful cutting of the specimens was performed with cutting wheels developed for non-ferrous metals. The specimens were hot mounted with Struers® PolyFast mounting powder. The subsequent planar grinding and polishing was performed with Struers® TegraPol-31/TegraForce-5 semiautomatic polishing machine using P240, P320, P800, P2000 and P4000 SiC papers. The final polish was carried out using Struers® MD-Chem cloth and OP-S polishing solution. The microstructure was revealed using Kroll's etchant (1 ml HF, 2 ml HNO<sub>3</sub> and 97 ml water).

The microstructural evaluation and characterization was carried out in light optical microscope. Large mosaic images were composed with the Microsoft Image Composite Editor.

### 5.3.2 Fractography

In papers 1 and 3, fractographic characterization has been carried out on the fracture surfaces of fatigue tested samples. In addition, tensile tested samples were investigated in paper 3. Initially, one of the two fractured halves was evaluated and if found necessary, the second half investigated as well. Fractographic evaluation was carried out in a LEO Gemini 1550 FEG scanning electron microscope.

By characterizing the topography of the fracture surface, information about the cause of crack initiation and fracture mechanisms can be revealed. Fatigue failure can be divided into different stages, i.e. crack initiation, crack propagation and final fracture. Figure 5.3 shows a crack initiation at a crack, a relatively flat crack propagation area around the initiation and the final fracture.

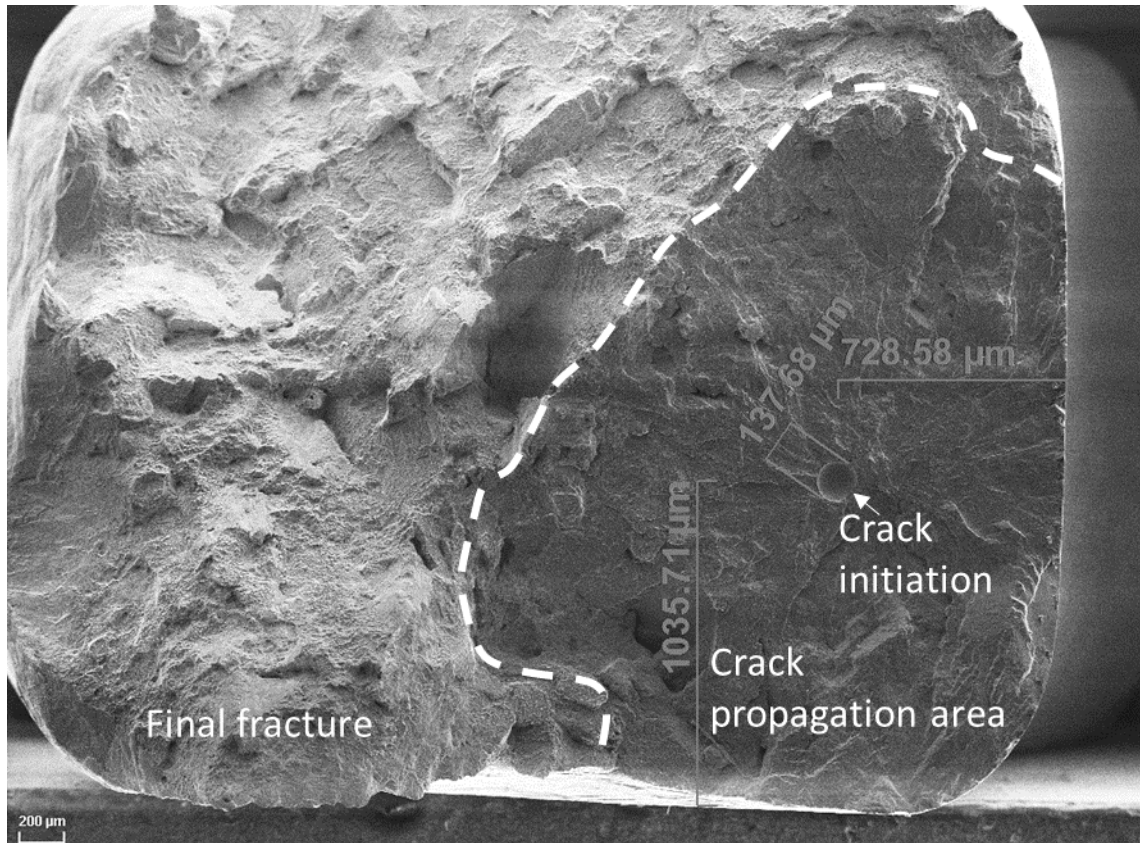


Figure 5.3. Fracture surface of a fatigue specimen. The size and the location of the defect that initiated the fatigue crack was measured.

## 5.4 Mechanical testing

The tensile testing and the low cycle fatigue testing were carried out by an ISO 17025 certified commercial mechanical testing laboratory. Below, the details for the performed mechanical testing are provided.

### 5.4.1 Tensile testing

The strain controlled tensile testing was performed according to the ASTM E8 at room temperature. The testing carried out at 250°C was performed according to ASTM E21. The tensile testing was performed in transverse direction to the weld.

## 5.4.2 Fatigue testing

The load controlled fatigue testing (paper 1 and 3) was performed according to ASTM E466 at room temperature and at 250°C. In paper 3, a set of polished and unpolished LBW specimens was also tested at 200°C.

Figure 5.4 shows the removal of external weld geometry from tensile test samples and LCF samples. The fatigue specimens were polished in order to study the effect of microstructure and internal defects. . In addition a set of unpolished laser beam welded samples were tested to influence from the external weld geometry.

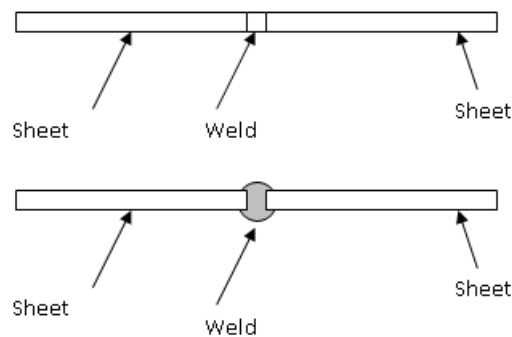


Figure 5.4. Schematic sketch of the LCF specimen geometry. Removal of the external weld geometry.

Specimens for fatigue testing were prepared in longitudinal and transverse direction to the weld as shown in Fig 5.5. Equal amount of samples were tested in both directions.

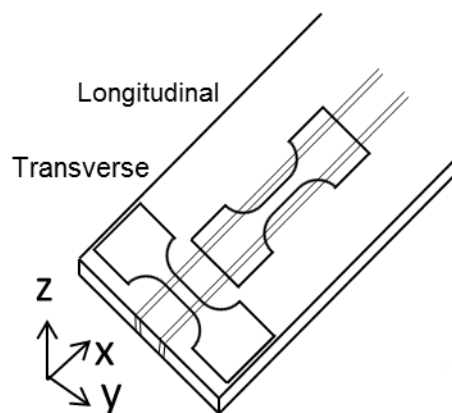


Figure 5.5. Schematic sketch of how the fatigue test specimens were cut out from the welded sheets.

### 5.4.3 Microhardness measurement

The microhardness measurements performed were performed with a Shimadzu HMV-200 –microhardness tester. In paper 1 a load of 300 g was used and in papers 2 and 3 a load of 500 g was used. A minimum of five indentation diameters was used as distance between the measurements. The hardness profiles presented in the papers are an average of 3 profiles across the welds at different depths.



## 6 Summary of appended papers/experimental results

### 6.1 Paper 1

#### Fatigue strength dependence on microstructure and defects in Ti-6Al-4V welds

In paper 1, the effect of defects and microstructure on fatigue strength of Ti-64 welds produced by PAW and TIG was studied. Both types of welds were fatigue tested at 250°C. Weld microstructure, fracture surfaces, crack initiation sites and internal defects such as porosity were studied using optical microscopy and SEM. The fatigue test specimens were machined to remove the external geometry of the welds in order to study the effects of internal defects and microstructure.

The metallographic investigation showed that the weld zones in TIG welds were wider and having larger prior- $\beta$  grains in the fusion zone indicating higher heat input compared to PAW. Electron back scatter diffraction (EBSD) technique was used to reveal the  $\alpha$  colonies which consist of similarly oriented  $\alpha$  plates which may be difficult to resolve in light optical microscope. Euler angle presentations of PAW and TIG welds (in Fig. 6.1) show that PAW mainly consists of basket weave structure whereas in TIG weld the amount of colony structure is higher. Microhardness was higher in the welds than in the base material and TIG welds had higher hardness than PAW.

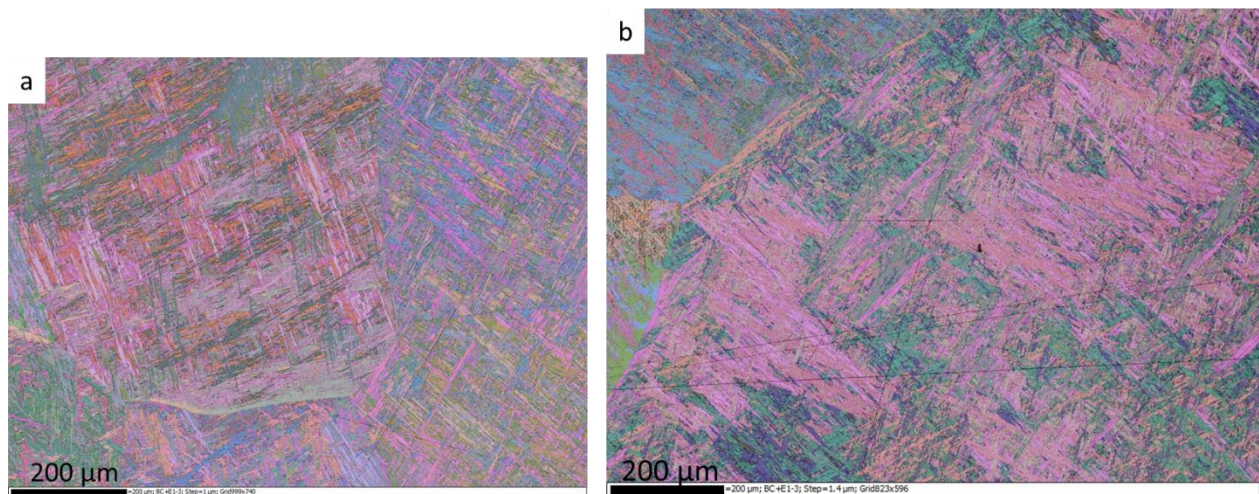


Figure 6.1. Euler angle presentation of a) PAW and b) TIG welds.

The fatigue test results are shown in Fig 6.2. The fatigue performance of TIG and PAW welds was found to be similar. Fractographic investigation was carried out in order to explain the large scatter in the fatigue results. Pores were found to initiate cracks in almost all samples. Large pores were found to have largest

influence on fatigue life regardless of their position. In addition, pores with a diameter larger than their distance from the surface had a large influence on fatigue life. The average pore size initiating a crack increased with the distance from the sample surface. In TIG welds, small pores were not found to initiate fracture when they were located inside the weld, while in PAW samples small internal pores were found to initiate cracks. TIG welds had larger pores than PAW welds, but TIG welds still performed similar or even better. This shows that the fatigue life of welds is affected by the weld microstructure. The microstructures of the investigated welds were similar in appearance but TIG welds had slightly higher hardness which may explain why the PAW seemed more sensitive to pores.

Sample geometry was found to expose some internal pores to the surface of the sample. It is possible that such pores would not influence the fatigue strength in a real component. Fatigue test specimens with this kind of exposed porosity had low fatigue life.

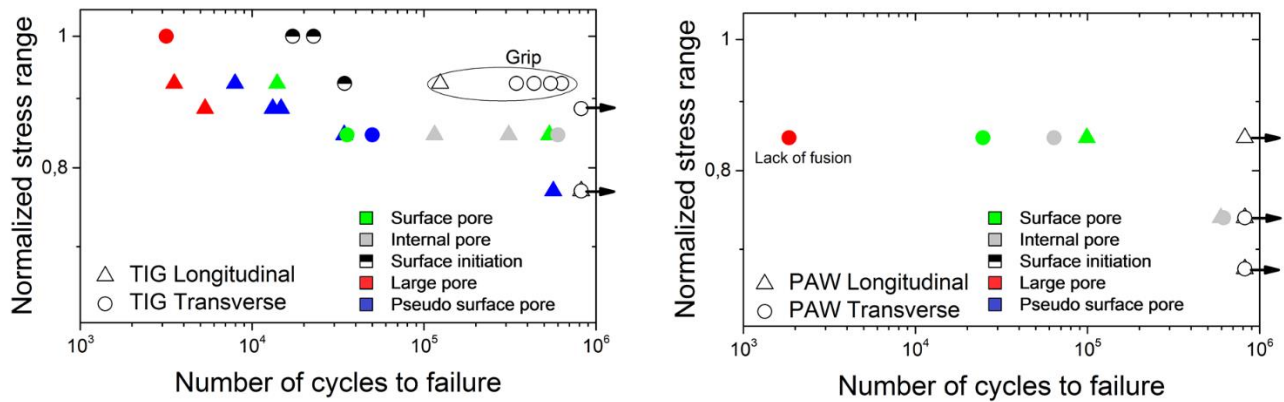


Figure 6.2. Fatigue test results of TIG and PAW welds. Color coding indicates the type of a crack initiation site.

## 6.2 Paper 2

### **TIG welding and laser welding of boron alloyed Ti-6Al-4V**

In paper 2, the microstructures and microhardness of TIG and laser welds performed on cast Ti-64 with boron contents of 0 wt.%, 0.06 wt.% and 0.11 wt.% were characterised. An addition of small quantities of boron to titanium alloys refines the solidification microstructure and  $\alpha$ - colony size dramatically. In TIG and laser welding, the boron addition was found to effect the morphology of prior  $\beta$  grains and  $\alpha$  plates in fusion zone and heat affected zone. The welding also affected the morphology and distribution of TiB particles. Boron addition is not found to have significant effect on microhardness in the welds.

In the conventional Ti-64 alloy without boron addition large prior  $\beta$  grains exist in the fusion zone and in the heat affected zone, whereas in the boron-doped alloys the prior  $\beta$  grains are found to be approximately 5 times smaller. In the heat affected zones of the boron-doped alloys incoherent TiB precipitates are distributed mainly along the prior  $\beta$  grain boundaries, inhibiting grain growth at elevated temperature and being the main reason for the grain refinement in the heat affected zone. In the fusion zone, TiB precipitates are found in stripes at interdendritic regions. Prior  $\beta$  grains are elongated and their size is refined by boron addition. The microstructure in the fusion zones and heat affected zones consists of fine acicular  $\alpha$ . Finely dispersed TiB precipitates in the fusion zone restrict the length of individual  $\alpha$  laths and the size of  $\alpha$  colonies as shown in Fig 6.2. The aspect ratio of  $\alpha$  plates is lower in the fusion zones of boron-alloyed welds in comparison to the fusion zone of conventional Ti-64 and the heat affected zone. The heat of the welding process alters the morphology of TiB particles. TiB particles are unaffected in the heat affected zone and appear to break up close to the fusion boundary. The size of the TiB precipitates is about 10 times smaller in the fusion zone than in the base material.

Boron addition refines the prior  $\beta$  grain size, reduces the aspect ratio of  $\alpha$  plates and the size of  $\alpha$  colonies, and minimizes the grain boundary  $\alpha$ . All these factors have been reported to contribute to the poor ductility of welded  $\alpha+\beta$  titanium alloys. Further work is needed to evaluate the mechanical properties of boron-alloyed welds and the effect on boron on formation of welding defects.

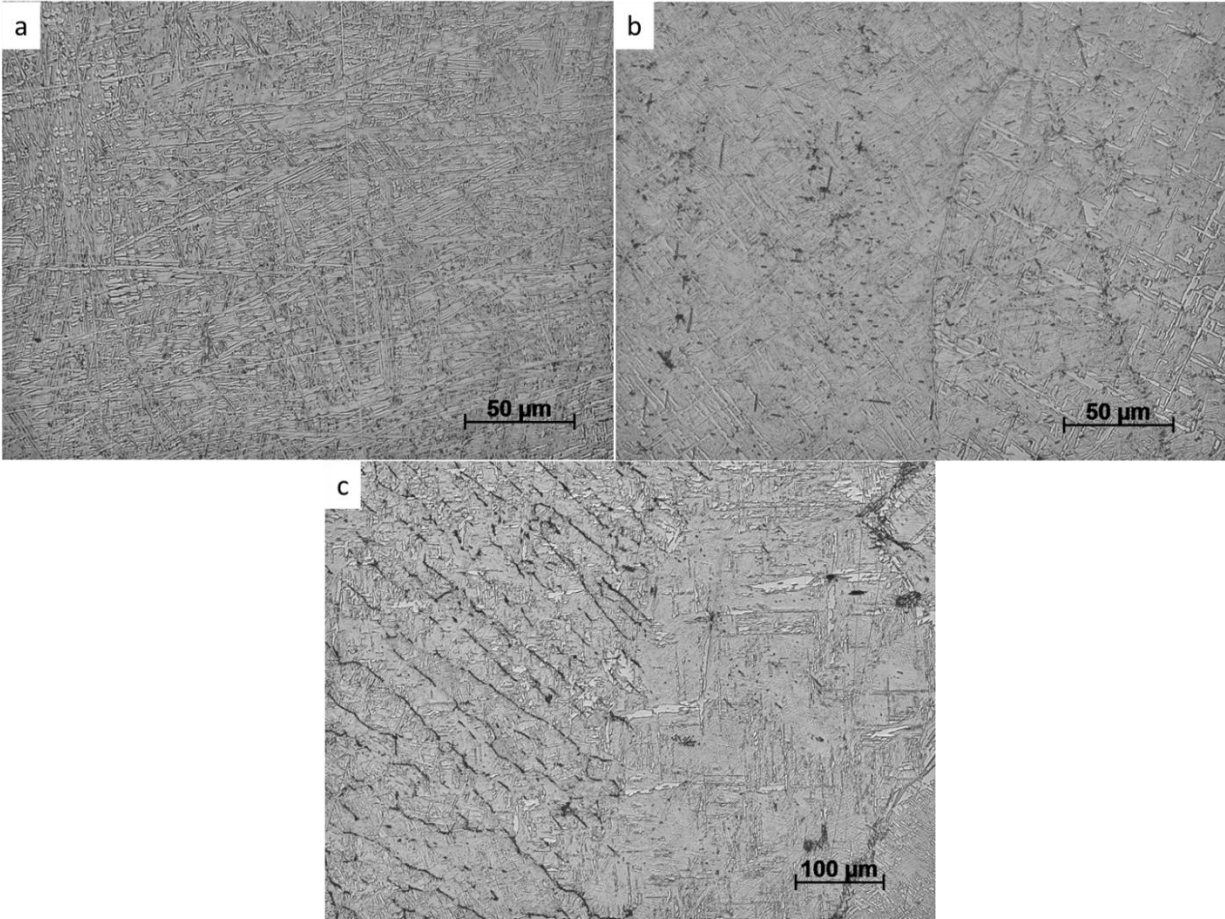


Figure 6.3. Micrographs of laser weld fusion zones on a) Ti-64, b) Ti-64-0.06B, and c) fusion boundary on Ti-64-0.11B

## 6.3 Paper 3

### **Comparing microstructure and mechanical properties of Ti-6Al-4V welds produced with different processes**

In paper 3 the effect of defects and microstructure on mechanical properties of Ti-64 welds produced by tungsten inert gas welding (TIG), plasma arc welding (PAW), electron beam welding (EBW) and laser beam welding (LBW) was studied. Load controlled fatigue tests and tensile tests were carried out at room temperature and at elevated temperature. The welds produced with EBW, LBW, TIG and PAW have different microstructures and different populations of defects in terms of their size and distribution. The effect of these aspects on mechanical properties under different testing conditions has been investigated.

Microstructural investigations showed that EBW and LBW produced narrower welds with finer microstructure. The microhardness of the welds was higher as compared to the base material. Despite the higher hardness of the welds, all the welds fractured in the fusion zone during tensile testing and fracture was found to be a combination of transgranular and intergranular fracture. The tensile ductility was lowered, and TIG and PAW showed the lowest ductility. The lower ductility may be related to coarser prior  $\beta$  grain size. Investigation of the LCF specimens by use of X-ray microscopy and fractography showed that EBW and PAW had least amount of porosity, whereas TIG welds had scattered porosity with larger average size. The investigated LBW sample revealed continuous porosity along the centerline of the weld together with occasional large pores.

Figure 6.4 shows the results of LCF tests carried out at 250°C with the type of crack initiation indicated by a unique symbol. Large defects have most detrimental effect on fatigue life on all stress ranges. At high stress ranges, cracks initiate easily and surface initiations dominate. At lower stress ranges, smaller defects can act as crack initiation sites, because cracks do not initiate and grow from the surface. At room temperature, the fatigue performance was found to be more sensitive to porosity.

EBW and LBW were found to have better fatigue performance than TIG and PAW. Almost all TIG and PAW specimens had crack initiation at a pore, whereas most EBW and LBW samples had a crack initiation at a defect-free surface. Only large pores and surface pores were found to initiate cracks in EBW and LBW. The finer microstructure in EBW and LBW improves resistance to micro crack initiation which contributes to better fatigue performance and makes them less sensitive to porosity.

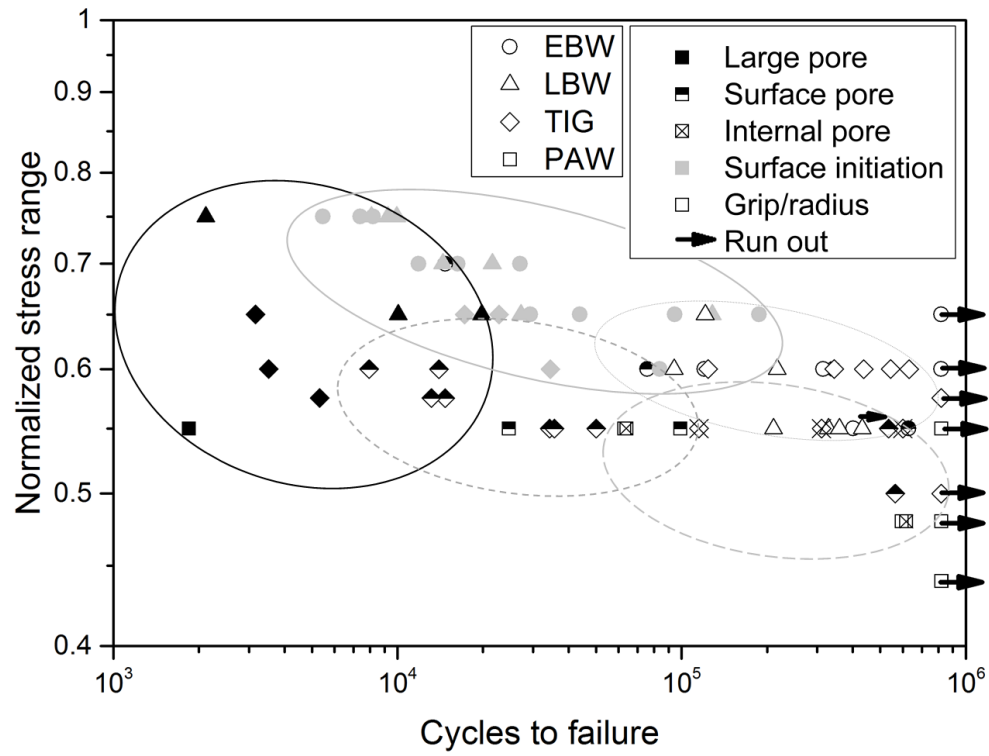


Figure 6.4. LCF results for welds produced by TIG, PAW, EBW and LBW at 250°C.

## 6.4 Conclusions

The aim of the work was to study what kind of microstructures and defects are formed in welding of titanium alloys with different welding processes and how these aspects affect the mechanical properties of the welds. The study showed that tungsten inert gas welding, plasma arc welding, laser beam welding and electron beam welding are all processes capable of creating high quality fusion welded joints in titanium alloys. The welds have different microstructures and different populations of defects in terms of their size and distribution. The welds produced by TIG and PAW had wider welds zones, coarser prior  $\beta$  grain structure and coarser intragranular microstructure. EBW and LBW welds were narrow and had very fine acicular intragranular microstructure. The microstructure of the welds could also be manipulated with alloy composition. A small boron addition was found to refine the prior  $\beta$  grain size, reduce the aspect ratio of  $\alpha$  plates and size of  $\alpha$  colonies and eliminate the grain boundary  $\alpha$ . All these factors have been reported to contribute to the ductility of welded  $\alpha+\beta$  titanium alloys. Fractographic investigation and X-ray microscopic investigation showed that TIG and LBW had more porosity with larger size than EBW and PAW.

The differences in the microstructures and defect distribution was found to have an effect on the mechanical properties. The finer microstructure of EBW and LBW contributed to higher tensile strength and tensile ductility of these welds. Finer microstructure has higher resistance to micro crack initiation and growth which contributed to better fatigue performance of EBW and LBW welds. The fatigue results showed large scatter and fractographic investigation showed that presence of large pores and surface pores lowered the fatigue life significantly. EBW and LBW welds seemed to be less sensitive to porosity, as most samples had crack initiation at the surface of the sample, whereas TIG and PAW had a crack initiation almost always at a pore. Small internal pores were more detrimental to fatigue life at room temperature than at elevated temperatures.





## 7 Future work

The results presented in this study has shed some more light on understanding the relationship between pore size and their distribution in different Ti-64 welds, and how these pores influence mechanical properties. More work is however needed to completely understand why the welded tensile test samples fractured in the weld zone and not in the base material, considering that the least hard material across all the different welds are the base metal. In future work an extended study on the boron alloyed Ti-64 welds is anticipated. Future complementing X-ray tomography investigations of welded Boron doped Ti-64 material are believed to be able to resolve if the Boron additions affects the amount and/or distribution of pores in the weld zone. Indications of this effect was found in the current work, but more weld volume materials needs to be investigated before any conclusions about these findings are justified. Further microstructural studies including quantification of microstructural features, including EBSD analysis, to characterize solidification microstructure in the fusion zone as well as study the morphology and stability of TiB particles, is also anticipated.



## 8 Acknowledgements

I would like to thank and express my sincere gratitude to my examiner Professor Uta Klement and supervisor Professor Robert Pederson for their guidance, patience and encouragement in the last three years. Your professional and personal support has been invaluable for the development of this work.

I would like to thank our research engineers: Dr. Eric Tam, Dr. Yiming Yao, Lars Hammar and Roger Sagdal for all the practical support. A special thanks goes to Dr. Kenneth Hamberg who introduced me to the world of fatigue fractures and metallographic preparation of titanium alloys.

I would also like to acknowledge GKN Aerospace Engine Systems for providing materials, welding experiments, mechanical testing, and expertise on which the current thesis is based on. NFFP (the Swedish National Program for Aeronautical Technology) is acknowledged for financial support of this PhD project.

I would like to thank my former and current colleagues at the Department of Materials and Manufacturing Technology for creating a friendly and motivating working environment.

I would like to thank all my friends for making my stay in Sweden unforgettable and the friends in Finland, I will not forget you.

My family and parents. I would not be here without you.



## References

- [1] R. R. Boyer, “An overview on the use of titanium in the aerospace industry,” *Materials Science and Engineering: A*, vol. 213, no. 1–2, pp. 103–114, Aug. 1996.
- [2] G. W. Meetham, Ed., *The Development of Gas Turbine Materials*. Dordrecht: Springer Netherlands, 1981.
- [3] F. H. S. Froes and M. A. Imam, “Cost Affordable Developments in Titanium Technology and Applications,” *Key Engineering Materials*, vol. 436, no. May, pp. 1–11, 2010.
- [4] M. J. Donachie, *Titanium A Technical Guide*, 2nd ed. ASM International, 2000.
- [5] G. Lütjering and J. C. William, *Titanium*. Springer-Verlag Berlin Heidelberg New York, 2003.
- [6] C. Leyens and M. Peters, *Titanium and titanium alloys : fundamentals and applications*. Wiley-VCH, 2003.
- [7] R. Pederson, R. Gaddam, and M.-L. Antti, “Microstructure and mechanical behavior of cast Ti-6Al-4V with addition of boron,” *Central European Journal of Engineering*, vol. 2, no. 3, pp. 347–357, 2012.
- [8] G. Singh, R. Gaddam, V. Petley, R. Datta, R. Pederson, and U. Ramamurty, “Strain-controlled fatigue in B-modified Ti-6Al-4V alloys,” *Scripta Materialia*, vol. 69, no. 9, pp. 698–701, 2013.
- [9] G. Singh, D. V. V Satyanarayana, R. Pederson, R. Datta, and U. Ramamurty, “Enhancement in creep resistance of Ti-6Al-4V alloy due to boron addition,” *Materials Science and Engineering A*, vol. 597, pp. 194–203, 2014.
- [10] S. Roy, S. Suwas, S. Tamirisakandala, D. B. Miracle, and R. Srinivasan, “Development of solidification microstructure in boron-modified alloy Ti-6Al-4V-0.1B,” *Acta Materialia*, vol. 59, no. 14, pp. 5494–5510, 2011.
- [11] S. Tamirisakandala, R. B. Bhat, J. S. Tiley, and D. B. Miracle, “Grain refinement of cast titanium alloys via trace boron addition,” *Scripta Materialia*, vol. 53, no. 12, pp. 1421–1426, 2005.
- [12] I. Sen, K. Gopinath, R. Datta, and U. Ramamurty, “Fatigue in Ti – 6Al – 4V – B alloys,” *Acta Materialia*, vol. 58, pp. 6799–6809, 2010.

- [13] M. J. Bermingham, D. Kent, H. Zhan, D. H. StJohn, and M. S. Dargusch, "Controlling the microstructure and properties of wire arc additive manufactured Ti-6Al-4V with trace boron additions," *Acta Materialia*, vol. 91, pp. 289–303, 2015.
- [14] ASM International. Handbook Committee., *ASM handbook, vol 6a*. ASM International, 1993.
- [15] S. Katayama, *Handbook of laser welding technologies*. Woodhead Publishing, 2013.
- [16] K. Weman, *Welding processes handbook*. Woodhead Pub, 2012.
- [17] C. S. Wu, L. Wang, W. J. Ren, and X. Y. Zhang, "Plasma arc welding: Process, sensing, control and modeling," *Journal of Manufacturing Processes*, vol. 16, no. 1, pp. 74–85, 2014.
- [18] C. L. Jenney, A. O'Brien, American Welding Society., and Welding Handbook Committee., *Welding handbook*. American Welding Society, 2001.
- [19] K. E. Easterling, *Introduction to the physical metallurgy of welding*. Butterworth Heinemann, 1992.
- [20] K. K. Murthy, N. B. Potluri, and S. Sundaresan, "Fusion zone microstructure and fatigue crack growth behaviour in Ti-6Al-4V alloy weldments," *Materials Science and Technology*, vol. 13, no. June, pp. 503–510, Jun. 1997.
- [21] T. Ahmed and H. J. Rack, "Phase transformations during cooling in alpha + beta titanium alloys," *Materials Science and Engineering A*, vol. 243, pp. 206–211, 1998.
- [22] S. K. Kar, "Modeling of mechanical properties in alpha/beta-titanium alloys," The Ohio State University, 2005.
- [23] A. B. Short, "Gas tungsten arc welding of  $\alpha + \beta$  titanium alloys: a review," *Materials Science and Technology*, vol. 25, no. 3, pp. 309–324, Mar. 2009.
- [24] F. X. Gil Mur, D. Rodríguez, and J. a. Planell, "Influence of tempering temperature and time on the  $\alpha'$ -Ti-6Al-4V martensite," *Journal of Alloys and Compounds*, vol. 234, no. 2, pp. 287–289, 1996.
- [25] K. K. Murthy and S. Sundaresan, "Fracture toughness of Ti-6Al-4V after welding and postweld heat treatment.pdf," *Welding journal*, vol. 76, no. 2, pp. 81–91, 1997.
- [26] X. J. Cao, G. Debaecker, M. Jahazi, S. Marya, J. Cuddy, and A. Birur, "Effect of Post-Weld Heat Treatment on Nd: YAG Laser Welded Ti-6Al-4V Alloy Quality," *Materials Science Forum*, vol. 638–642, pp. 3655–3660, 2010.
- [27] A. S. H. Kabir, X. Cao, J. Gholipour, P. Wanjara, J. Cuddy, A. Birur, and M. Medraj, "Effect of Postweld Heat Treatment on Microstructure, Hardness, and Tensile Properties of Laser-Welded Ti-6Al-4V," *Metallurgical and Materials Transactions A*, vol. 43, no. 11, pp. 4171–4184, Jun. 2012.

- [28] T. Matsumoto, N. Fukuda, Y. Kondo, A. Ohmori, K. Inoue, and Y. Arata, "Study on prevention of welding defects in high power CO<sub>2</sub> laser materials processing," *Journal of Laser Applications*, vol. 11, no. 6, p. 258, 1999.
- [29] L. S. Smith and M. F. Gittos, "A review of Weld Metal Porosity and Hydride Cracking in Titanium and Its Alloys, report 658," The Welding Institute, 1998.
- [30] T. Khaled, "An Investigation of Pore Cracking in Titanium Welds," *The Weld*, vol. 3, no. June, 1994.
- [31] M. M. Alam, J. Powell, a. F. H. Kaplan, J. Tuominen, P. Vuoristo, J. Miettinen, J. Poutala, J. Näkki, J. Junkala, and T. Peltola, "Surface pore initiated fatigue failure in laser clad components," *Journal of Laser Applications*, vol. 25, no. 3, p. 32004, 2013.
- [32] J. Schijve, *Fatigue of Structures and Materials*. Springer Science+Business Media, B.V., 2009.
- [33] F. Karimzadeh, M. Salehi, A. Saatchi, and M. Meratian, "Effect of microplasma arc welding process parameters on grain growth and porosity distribution of thin sheet Ti6Al4V alloy weldment," *Materials and Manufacturing Processes*, vol. 20, no. 2, pp. 205–219, 2005.
- [34] J. Blackburn, *Laser welding of metals for aerospace and other applications*. Woodhead Publishing Limited, 2011.
- [35] J. Huang, "The characterisation and modelling of porosity formation in electron beam welded titanium alloys," The University of Birmingham, 2011.
- [36] A. Matsunawa, M. Mizutani, S. Katayama, and N. Seto, "Porosity formation mechanism and its prevention in laser welding," *Welding International*, vol. 17, no. 6, pp. 431–437, Jun. 2003.
- [37] A. Matsunawa, J.-D. Kim, N. Seto, M. Mizutani, and S. Katayama, "Dynamics of keyhole and molten pool in laser welding," *Journal of Laser Applications*, vol. 10, no. 6, p. 247, 1998.
- [38] A. F. H. Kaplan, M. Mizutani, and S. Katayama, "On the Mechanism of pore formation during keyhole laser spot welding," in *Proceedings of the SPIE*, 2003, vol. 4831, pp. 186–191.
- [39] J. E. Blackburn, "Understanding porosity formation and prevention when welding titanium alloys with 1  $\mu\text{m}$  wavelength laser beams," The University of Manchester, 2011.
- [40] S. Katayama, Y. Kobayashi, M. Mizutani, and A. Matsunawa, "Effect of vacuum on penetration and defects in laser welding," *Journal of Laser Applications*, vol. 13, no. 5, p. 187, 2001.
- [41] N. Gouret, G. Dour, B. Miguet, E. Ollivier, and R. Fortunier, "Assessment of the Origin of Porosity in Electron-Beam-Welded TA6V Plates," *Metallurgical and Materials Transactions A*, vol. 35, no. March, pp. 879–889, 2004.

- [42] W. W. Duley, *Laser welding*. Wiley, 1999.
- [43] X. Cao and M. Jahazi, “Effect of welding speed on butt joint quality of Ti–6Al–4V alloy welded using a high-power Nd:YAG laser,” *Optics and Lasers in Engineering*, vol. 47, no. 11, pp. 1231–1241, 2009.
- [44] N. K. Babu and S. G. S. Raman, “Influence of current pulsing on microstructure and mechanical properties of Ti–6Al–4V TIG weldments,” *Science and Technology of Welding and Joining*, vol. 11, no. 4, pp. 442–447, 2006.
- [45] S. Sundaresan, G. D. Janaki Ram, and G. Madhusudhan Reddy, “Microstructural refinement of weld fusion zones in  $\alpha$ – $\beta$  titanium alloys using pulsed current welding,” *Materials Science and Engineering: A*, vol. 262, no. 1–2, pp. 88–100, 1999.
- [46] K. K. Murthy, N. B. Potluri, and S. Sundaresan, “Fusion zone microstructure and fatigue crack growth behaviour in Ti-6Al-4V alloy weldments,” *Materials Science and Technology*, vol. 13, no. June, pp. 503–510, 1997.
- [47] J. Oh, N. J. Kim, S. Lee, and E. W. Lee, “Correlation of fatigue properties and microstructure in investment cast Ti-6Al-4V welds,” *Materials Science and Engineering A*, vol. 340, pp. 232–242, 2003.
- [48] T. Mohandas, M. Srinivas, and V. V. Kutumbarao, “Effect of post-weld heat treatment on fracture toughness and fatigue crack growth behaviour of electron beam welds of a titanium (alpha+beta) alloy,” *Fatigue and Fracture of Engineering Materials and Structures*, vol. 23, no. 1, pp. 33–38, 2000.
- [49] M. M. Salama, “Fatigue Crack Growth Behavior of Titanium Alloy Ti-6Al-4V and Weldment,” *Journal of Offshore Mechanics and Arctic Engineering*, vol. 123, no. 3, p. 141, 2001.
- [50] J. Ault, J. Pillers, and S. Veeck, “The GTAW of Ti-6Al-4V castings and its effect on microstructural and mechanical properties,” *Jom*, vol. 57, no. November, pp. 62–65, 2005.
- [51] N. E. Dowling, *Mechanical behavior of materials : engineering methods for deformation, fracture, and fatigue*. Pearson/Prentice Hall, 2007.
- [52] S. Suresh, *Fatigue of materials*. Cambridge University Press, 1998.
- [53] S. J. Maddox, *Fatigue strength of welded structures*. Abington Publishing, 1991.
- [54] L. Smith, M. Gittos, and P. Threadgill, “High quality and productivity joining processes and procedures for titanium risers and flowlines,” in *Titanium Risers and Flowlines*, 1999.



- [55] S. J. Maddox and S. J., "Recent advances in the fatigue assessment of weld imperfections," *Welding journal*, vol. 72, pp. 42–51, 1993.
- [56] G. M. Peshak and D. V. Lindh, "The Influence of Weld Defects on Performance," *Welding Journal (Research Supplement)*, no. February, 1696.
- [57] M. Shirani and G. Härkegård, "Damage tolerant design of cast components based on defects detected by 3D X-ray computed tomography," *International Journal of Fatigue*, vol. 41, pp. 188–198, 2012.
- [58] S. Tammis-Williams, J. Donoghue, P. J. Withers<sup>1</sup>, I. Todd, and P. B. Prangnell, "Predicting the Influence of Porosity on the Fatigue Performance of Titanium Components Manufactured by Selective Electron Beam Melting," in *Proceedings of the 13th World Conference on Titanium*, 2015, pp. 1447–1452.
- [59] J. Z. Yi, Y. X. Gao, P. D. Lee, H. M. Flower, and T. C. Lindley, "Scatter in fatigue life due to effects of porosity in cast A356-T6 aluminum-silicon alloys," *Metallurgical and Materials Transactions A*, vol. 34, no. 9, pp. 1879–1890, 2003.
- [60] U. Zerbst, M. Madia, and H. T. Beier, "A model for fracture mechanics based prediction of the fatigue strength: Further validation and limitations," *Engineering Fracture Mechanics*, vol. 130, pp. 65–74, 2014.
- [61] Z. Xu, W. Wen, and T. Zhai, "Effects of pore position in depth on stress/strain concentration and fatigue crack initiation," *Metallurgical and Materials Transactions A: Physical Metallurgy and Materials Science*, vol. 43, no. 8, pp. 2763–2770, 2012.
- [62] J. Fan, D. L. McDowell, M. F. Horstemeyer, and K. Gall, "Cyclic plasticity at pores and inclusions in cast Al-Si alloys," *Engineering Fracture Mechanics*, vol. 70, pp. 1281–1302, 2003.
- [63] Y. Murakami, "Material defects as the basis of fatigue design," *International Journal of Fatigue*, vol. 41, pp. 2–10, Aug. 2012.